Carbon Letters (2020) 30:123–132
https://doi.org/10.1007/s42823-019-00089-x

Online ISSN 2233-4998
Print ISSN 1976-4251

ORIGINAL ARTICLE

High-efficiency adsorption for both cationic and anionic dyes using graphene nanoribbons formed by atomic-hydrogen induced single-walled carbon nanotube carpets

Yan Gao[1,2,3] · Xilong Liang[2,3] · Shuangping Han[2,3] · Liang Wu[1] · Guofeng Zhang[2,3] · Chengbing Qin[2,3] · Shanxia Bao[1] · Qiang Wang[1] · Lele Qi[1] · Liantuan Xiao[2,3]

Received: 27 November 2018 / Revised: 25 June 2019 / Accepted: 8 July 2019 / Published online: 29 August 2019

Abstract

Carbonaceous materials are considered as potential adsorbents for organic dyes due to their unique structures which provide high aspect ratios, hydrophobic property, large efficient surface area, and easy surface modification. In this work, graphene nanoribbons (GNRs) were prepared by atomic hydrogen-induced treatment of single-walled carbon nanotube (SWCNTs), which inspire the idea of cutting and unzipping the SWCNTs carpets with the modified in molecules prevent because of the unfolding of the side-walls. The unfolded spaces and uniform vertical arrangement not only enhance the active surface area, but also promote the electrostatic and π–π interactions between dyes and GNRs. The improved adsorption capacity of GNRs beyond original SWCNTs can be determined by the adsorption kinetics and isotherm, which are evaluated through adsorption batch experiments of the typical cationic methylene blue (MB) and anionic orange II (OII) dye, respectively. It is shown that the adsorption kinetics follow a pseudo second-order model while the adsorption isotherm could be determined by Langmuir model. The results reveal that the maximum adsorption capacities of GNRs for MB and OII are 280 and 265 mg/g, respectively. The GNRs present the highly efficient, cost effective, and environmental friendly properties for the commercial applications of wastewater treatment.

Graphic abstract

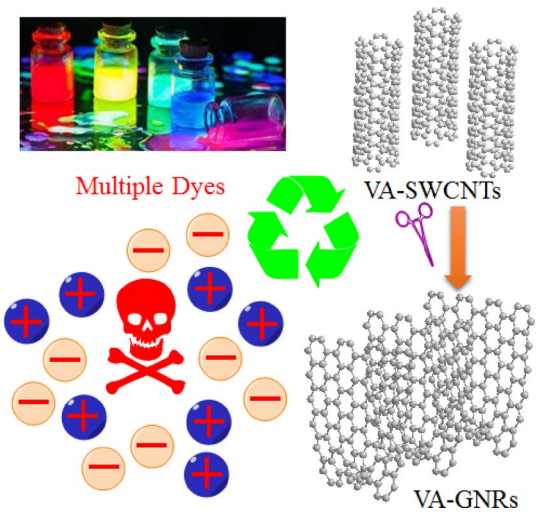

Keywords Atomic hydrogen treatment · Graphene nanoribbons · Organic dyes adsorption

Extended author information available on the last page of the article

1 Introduction

Pollution of ground and surface water with composite dyes has become one of the serious global environmental problems due to rapidly developing industries, which have endangered all living on the earth [1, 2]. Organic dyes, as one of the most important contaminants of wastewater, are mainly derived from the textile, printing, gasoline, leather tanning, food industries and so on [3]. It is known that more than hundreds of dyes are discharged in sewage water. Most of dyes possibly constitute the aromatic molecular structures, such as toluene, benzene, xylene, anthracene, naphthalene, etc. [4]. These structures lead them stable to the heat, photodegradation, oxidizing and biodegradation [5, 6].

In the past decade, the effective applications of the carbon nanotubes for the removal of individual cationic or anionic dyes have been investigated [7–22]. Yao et al. [23] reported the high adsorption capacity of typical cationic methylene blue (MB) onto single-walls carbon nanotube (SWCNTs). Konick et al. [24] proved that the magnetic multi-walled carbon nanotube nanocomposite can be considered as a high-efficient adsorber for anionic orange II (OII), which was treated as a typical anionic dye. Furthermore, other abundant carbonic materials such as activated carbon [25–28], graphene [29] and graphene oxide [30–32] have been used worldwide for commercial applications of dye adsorption. Ramesha et al. have shown that both graphene and graphene oxide can act as effective adsorbents toward anionic and cationic dyes from aqueous solutions, respectively. Rodríguez et al. [33] use multi-walled carbon nanotubes (MWCNTs) to product the carbon nanofibers (CNF) as adsorbents to investigate the adsorption of cationic MB and anionic OII simultaneously. Functionalized CNTs are naturally hydrophilic, which lead to the increased adsorption capacities for both cationic and anionic dyes from the wastewater due to the existence of corresponding electrostatic property for suitable functional groups on the surface. Robati et al. [34] performed the functionalized MWCNTs with a higher surface area and then reported a higher MB adsorption activity. Mishra et al. [35] used functionalized MWCNTs for removing three different types of organic dyes effectively [36]. However, the potential toxicity of functional groups may pollute and damage the water bodies.

Herein we demonstrate the high efficiency adsorption for both cationic and anionic dyes simultaneously using the atomic hydrogen treatment of vertically arranged single-walled carbon nanotubes (VA-SWCNTs). The produced graphene nanoribbons (VA-GNRs), which retain uniform vertical arrangement structure based on the completely unzipped VA-SWCNTs, can act as a novel adsorbent. Our study inspires the idea of cutting and unzipping the VA-SWCNT carpet which the modified in molecules prevent because of the unfolding of the side-walls. The large unfolded spaces and the vertically uniform structure both increase the active surface area as well as promote the π–π and electrostatic interaction between dyes and VA-GNRs.

2 Experimental section

2.1 Preparation of VA-GNR

Figure 1 demonstrates the diagrammatic cutting and unzipping process of the VA-SWCNTs carpet. First, according to the previous literature [37, 38], VA-SWCNTs were grown on a clean silicon substrate. Second, atomic hydrogen treatment, which used a mixture of H_2, H_2O and CH_4 at 25 Torr and 850 °C upon the samples, was carried out for certain time. The details of this treatment can be found in supporting information and the previous work [39]. As displayed

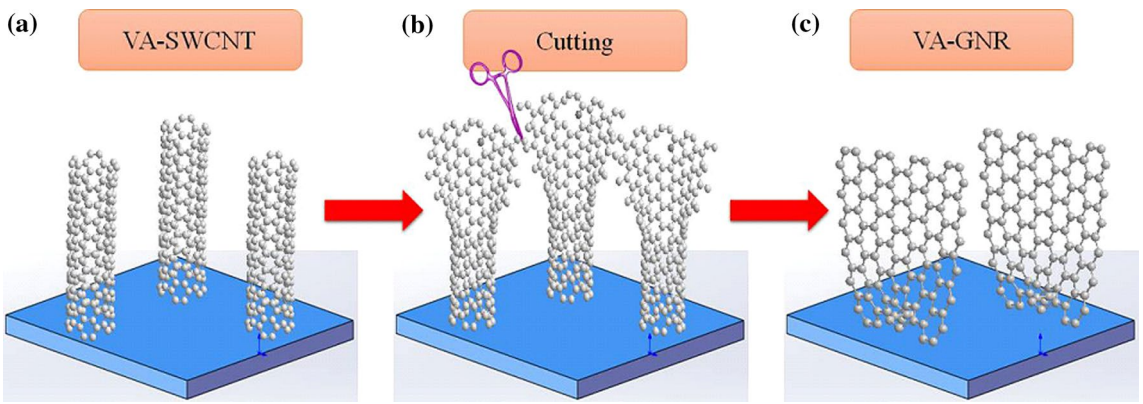

Fig. 1 Schematic representation of the reaction involved in the atomic hydrogen treatment of a vertically arranged single-walled carbon nanotubes (VA-SWCNTs) carpet. **a** VA-SWCNTs are first grown on a silicon substrate. **b** Teepee structure which formed by transverse cut and longitudinally unzip VA-SWCNTs. **c** Formed vertically arranged graphene nanoribbons (VA-GNRs) by atomic hydrogen treatment

in Fig. 1b, with atomic hydrogen treatment for 2 h, the top structure of the sample becomes open due to surface etching. Finally, the VA-GNRs were obtained with 4 h atomic hydrogen treatment to prepare VA-SWCNTs, as shown in Fig. 1c. Thus, VA-SWCNTs are laterally cut and vertically unzipped to form GNRs successfully.

2.2 Sample characterization

The scanning electron microscope (SEM) images of our sample are shown in Fig. 2. The as-grown VA-SWCNTs carpet demonstrates a large density on the flat surfaces and orderly occupied spread the whole substrate, as shown in Fig. 2a. Figure 2b presents the SEM image of the sample after treatment with atomic hydrogen for 2 h. The shorter fragments flock together to present a Native American "teepee" structure [40]. This phenomenon proves that the VA-SWCNTs are successfully laterally cut and vertically unzipped. Figure 1c presents the SEM image of VA-GNRs after treatment for 4 h, which reveals that VA-SWCNTs have been etched layer by layer, starting from top to the bottom of the carpet. The side view shows that the samples became cruder with some uniformly distributed stomas, which is more beneficial for wastewater adsorption and filtration accessibility. The middle space between each produced GNRs keeps growing as the increasing of treatment time. Meanwhile, the top bundle structures are formed on the ribbon layer.

Transmission electron microscope (TEM) images of SWCNTs and GNRs are shown in Fig. 3. The originally cylindrical nanotubes are demonstrated in Fig. 3a. Due to the atomic etching effects, Fig. 3b shows the open edge on the SWCNTs after the atomic hydrogen treatment for 2 h, where the effectively increased surface area clearly displays in unzipped layer of SWCNTs. For extending the hydrogen treatment time as well as contrasting to the traditional cylindrical nanotubes, the GNRs are expanded and flattened, as shown in Fig. 3c. The graphene nanoribbons with collapse and fission process show higher aspect ratio ribbons.

Atomic force microscope (AFM) characterization was also carried out to demonstrate the structural changes in the SWCNTs, as shown in Fig. 4. The height is about 2.1 nm, which indicates the typical height of SWCNTs. Figure 4c shows typical AFM image of GNRs prepared from VA-SWCNTs carpet with atomic hydrogen treatment. A long carbon nanotube bundle is connected to a graphene nanoribbon, which reveals bilayer GNRs with the thickness ranging from 3 to 5 nm (shown in Fig. 4d). This is also suggesting a complete transformation of 1.5–3 nm diameter SWCNTs to two-layer GNRs, strikingly similar to the dimensions of high-quality graphene prepared by chemical vapor deposition (CVD) methods [41].

The quantized characterizations for VA-SWCNTs and VA-GNRs are also demonstrated. Figure 5a presents the Raman spectra of the samples before and after treatment, which indicates that the resonance peaks of Raman remain unchanged. X-ray diffraction (XRD) patterns of the VA-SWCNTs and VA-GNRs samples are shown in Fig. 5b, which indicates that there is no other impurity in the samples. The (002) peak becomes narrow and shifts slightly to higher 2θ. The (101) peak is sharpened and changed to the main peak after atomic hydrogen treatment, which is

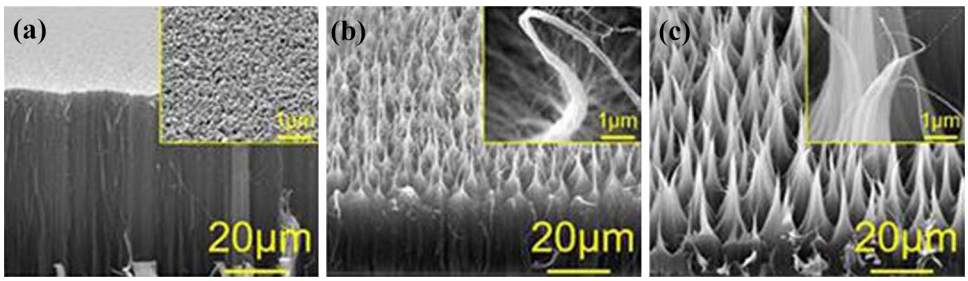

Fig. 2 The SEM micrograph of **a** pristine VA-SWCNTs; **b** atomic hydrogen treatment for 2 h and **c** for 4 h, respectively

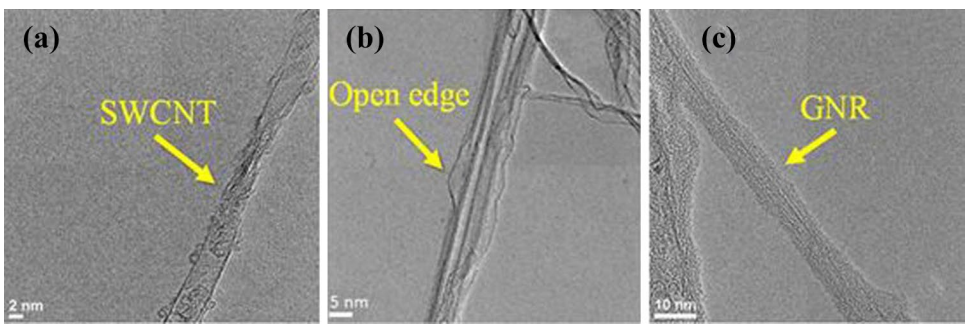

Fig. 3 TEM image of **a** pristine VA-SWCNTs; **b** atomic hydrogen treatment for 2 h and **c** for 4 h, respectively

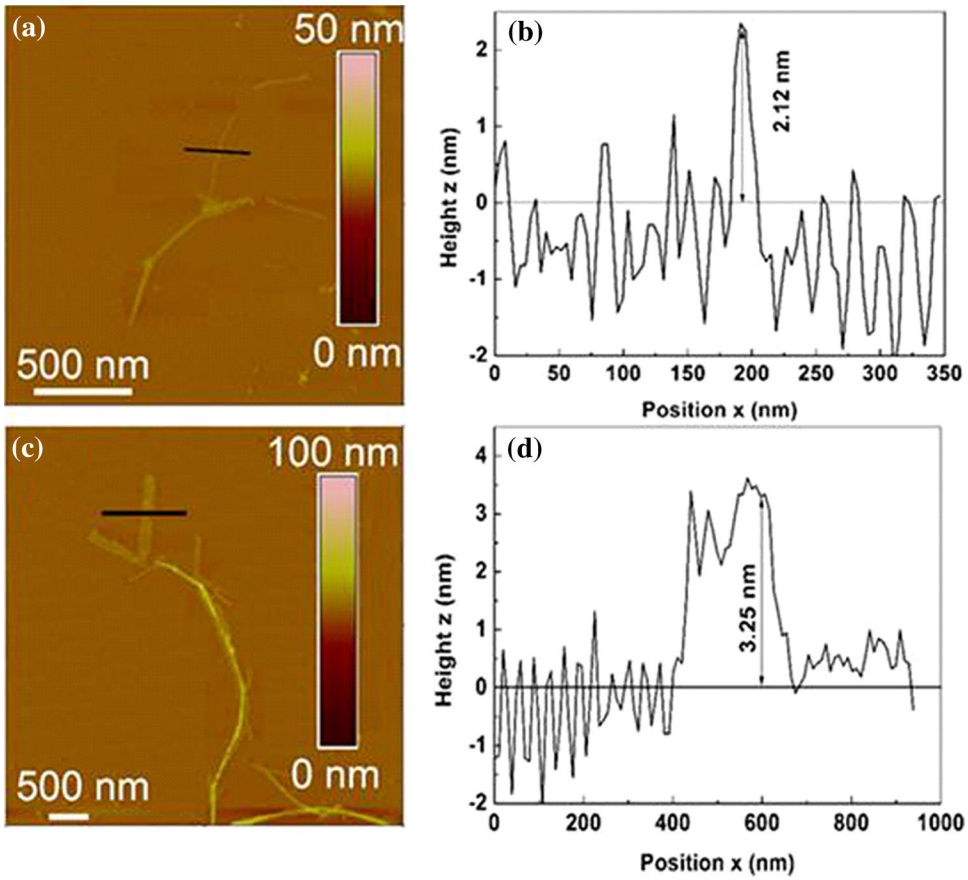

Fig. 4 AFM characterization of **a**, **b** an individual nanostructure from the VA-SWCNTs and **c**, **d** after atomic hydrogen treatment

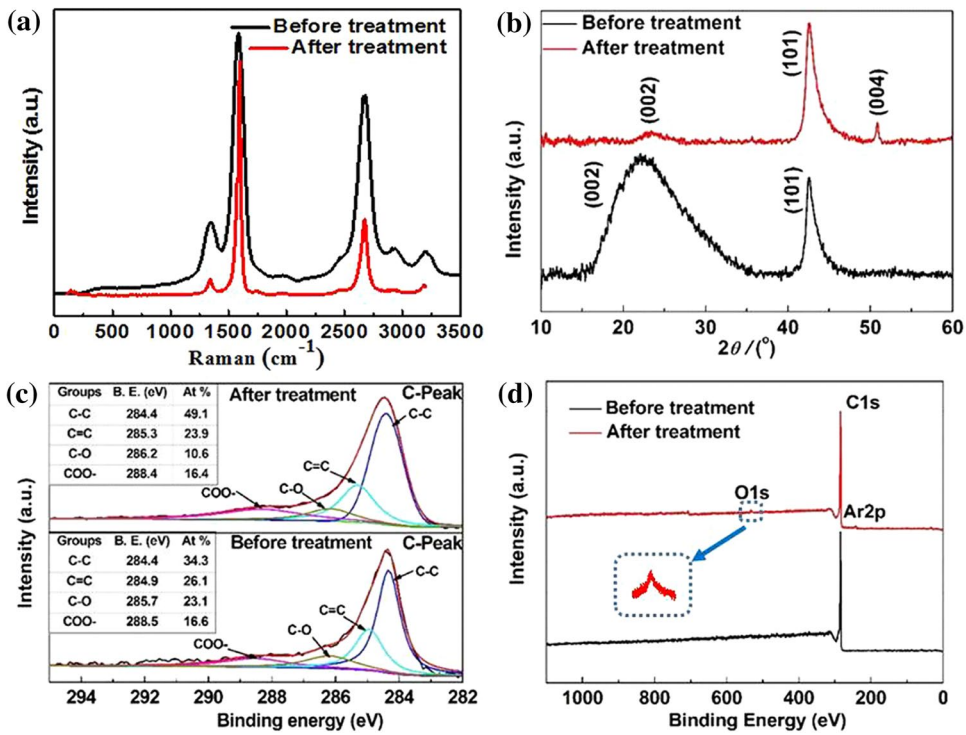

Fig. 5 **a** Raman spectra, **b** XRD patterns and **c**, **d** XPS spectra of as-prepared VA-SWCNTs carpets before and after atomic hydrogen treatment

attributed to the removal of graphitic carbon impurities by atomic hydrogen [42, 43]. Figure 5c, d depicts the X-ray photoelectron spectroscopy (XPS) of VA-SWCNTs and VA-GNRs carpet, and the main parameters are presented in the insert table. The deconvolution of C1s spectra is split into four peaks: C–C, C=C, C–O and C=O. As exhibited in Fig. 5c, the atomic percentage in the C1s spectra of graphitic carbon (C–C) on the VA-SWCNT surface is 34.3%. After atomic hydrogen treatment for 4 h, the percentage of C–C increases to 49.1%. The longer the treatment time, the stronger the etching effect of atomic hydrogen, because of the formation of more graphitic carbon (C–C bond). Besides, Fig. 5d shows the slight increase in oxygen signal after the atomic hydrogen treatment, which could be attributed to physis-orbed oxygen [44].

3 Results and discussion

3.1 Adsorption kinetics

The adsorption capacities of cationic dye MB and anionic dye OII on VA-SWCNTs and VA-GNRs have been investigated, respectively. The concentrations of MB and OII were measured by UV–Vis spectrophotometer (Ocean Optics May2000Pro), determining their maximum absorbance at the wavelengths of 510 and 662 nm, respectively. On account of Lambert–Beer's law, we established the calibration plots of dye concentrations. The detailed adsorbed process were performed by mixing 2 mg VA-SWCNTs or VA-GNRs with 20 mL samples of MB or OII solution with different initial concentrations in the sealed bottles, which were shaken for 5 h in a thermostatic water bath at 20 °C. The adsorption capacity is calculated using the following equation:

$$q_e = \left(\frac{C_0 - C_e}{m}\right) \times V, \tag{1}$$

where C_0 and C_e are initial and equilibrium concentrations (24 h) of MB or OII (mg/L), respectively, m is the mass of adsorbent (g) and V is volume of the solution (L).

On account of investigating the kinetic process of the adsorption, the adsorption capacities are demonstrated as a function with the equilibrium time of dye adsorption. The residual concentration of dye solution C_t is determined with the treatment time of 5, 10, 15, 20, 40, 90, 180, 330, 450, 570, 750, 1440, 1800 and 2880 min, respectively. The adsorption capacities q_t for adsorbed dyes onto VA-SWCNTs or VA-GNRs are determined according the following equation:

$$q_t = \left(\frac{C_0 - C_t}{m}\right) \times V, \tag{2}$$

where C_t is the concentration of residual dye solution.

Figure 6 presents the adsorption capacities of MB (Fig. 6a–c) and OII (Fig. 6d–f) changing with the adsorbed time from 5 to 2880 min for VA-SWCNTs and VA-GNRs, respectively. As expected, the results reveal that both the adsorption capacities of MB and OII on VA-GNRs are much higher than that of VA-SWCNTs. Furthermore, the adsorption capacity is rapidly increased in the first 5 min of both MB and OII dyes onto VA-GNRs, which achieves the equilibrium condition under 30 min. The higher adsorption capacity and faster adsorption rate are caused by the π–π electron donor–acceptor interaction and electrostatic attraction. These characteristics make both anionic and cationic dyes interact immediately contacting with the surface of VA-GNRs, unlike the VA-SWCNTs.

To investigate the processes and parameters of adsorption kinetic, two different kinetic models: (1) pseudo-second order model and (2) intraparticle diffusion model were used to fit the experimental data, respectively.

The pseudo-second order model is usually carried out for describing the chemisorption process with a rate-limiting step [45], represented as follows:

$$\frac{t}{q_t} = \frac{t}{q_e} + \frac{1}{k_2 q_e^2}, \tag{3}$$

where q_e and q_t show the adsorption amount of dyes at equilibrium condition and time t, respectively. The parameter k_2 in g/(mg min) reveals the rate constant of the pseudo-second order kinetic model. Specifically, the value V_0 expresses the initial adsorption rate [3, 46], where

$$V_0 = k_2 q_e^2. \tag{4}$$

Table 1 shows the linearly fitting parameters of t/q_t against time t. The linear correlation coefficients, $R^2 > 0.99$, suggest that both MB and OII absorbed onto VA-GNRs and VA-SWCNTs follow the pseudo-second order model. Note that the equilibrium adsorption capacities of MB and OII on VA-GNRs are 2.5- and 4.2-fold higher than that on VA-SWCNTs, respectively.

The intraparticle model is commonly applied to demonstrate the conceivable diffusion mechanism [47], which depicts the consecutive diffusion processes of dyes pass the periphery layer of VA-SWCNTs and VA-GNRs. The following equation expresses the diffusion process:

$$q_t = k_p t^{\frac{1}{2}} + C, \tag{5}$$

where k_p in mg/(g min$^{1/2}$) and C in mg/g is the intraparticle diffusion rate constant and the intercept, respectively. It reveals that the kinetics process is affected by the thickness of the periphery layer, which means that the C is increased

as the larger periphery-layer effect. Figure 6c, f presents the plots of q_t vs. $t^{1/2}$ and their fitting lines corresponding to MB and OII, respectively. The calculated parameters have been presented in Table 2. Although the correlation coefficients are briefly lower than that of pseudo-second order model; however, as presented in Table 2, both k_p and C corresponding to VA-GNRs are much higher than VA-SWCNTs, either MB or OII.

3.2 Adsorption isotherm

Herein the adsorption isotherm reveals the relationship between the residual dyes concentrations and adsorption capacity at equilibrium condition (C_e). It provides the detailed information about surface properties, adsorption mechanisms, and appetency of adsorbent for the dyes. We investigate the adsorption capacity of different initial concentrations of both MB and OII dyes onto VA-SWCNTs and VA-GNRs. Figure 7 demonstrates the adsorption capacities varying as the residual concentrations of equilibrium condition, which were performed after shaking the solution

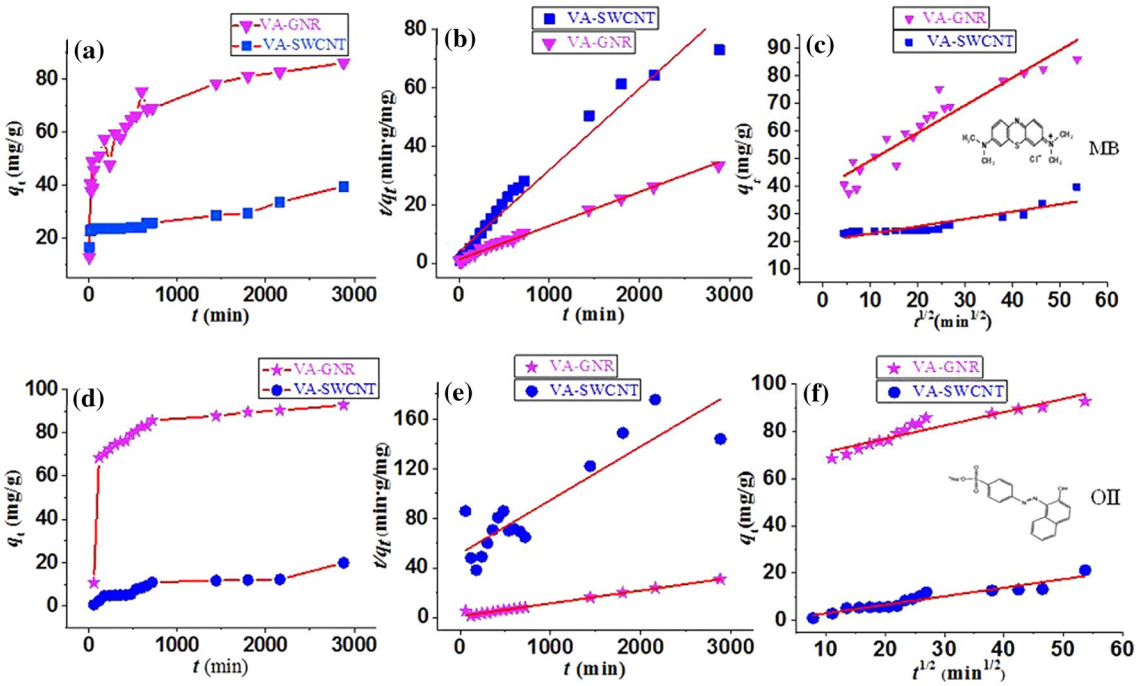

Fig. 6 Adsorption kinetics of **a** MB and **d** OII on VA-SWCNTs and VA-GNRs, respectively. **b**, **e** and **c**, **f** are the plots of pseudo-second order and intraparticle diffusion models for the MB and OII adsorption on VA-SWCNTs and VA-GNRs, respectively

Table 1 Parameters of pseudo-second order kinetic models

Pseudo-second order	MB	SWCNT	GNR	OII	SWCNT	GNR
	q_e	35.7	86.4	q_e	23.1	96.8
	V_0	0.13	1.49	V_0	0.01	0.75
	k_2	1.05×10^{-4}	2.0×10^{-4}	k_2	0.3×10^{-4}	0.8×10^{-4}
	R^2	0.96	0.99	R^2	0.81	0.99

Table 2 Parameters of interparticle diffusion kinetic model

Interparticle diffusion kinetic model	MB	SWCNT	GNR	OII	SWCNT	GNR
	k_{p1}	2×10^{-1}	1.0×10^{0}	k_{p1}	3×10^{-1}	5×10^{-1}
	C_1	22	39.4	C_1	4.2	65.7
	R^2	0.85	0.93	R^2	0.92	0.89

of mixture for 24 h at room temperature. Note that VA-GNRs display much large adsorption capacity than that of VA-SWCNTs.

To investigate the maximum adsorption capacity and the relative mechanism, Langmuir and Freundlich isotherm models are used to analyze the experimental data. It reveals no interaction between the dye molecules and adsorbent by Langmuir model, which performed the adsorption process on a tidily flat surface [8, 48]. It can be represented as follows:

$$\frac{C_e}{q_e} = \frac{C_e}{q_{max}} + \frac{1}{q_{max}}\frac{1}{K_L}, \tag{6}$$

where q_{max} is the maximum adsorption capacity in mg/g, in accordance with the whole monolayer coverage; K_L in L/mg is the Langmuir constant, relative to the energy of adsorption and affinity of the binding sites. Table 3 shows all the parameters of Langmuir model, which are determined by linearly fitting the plots of C_e/q_e against C_e, as shown in Fig. 7b, e. For both MB and OII, the correlation coefficients R^2 are greater than 0.9 for VA-SWCNTs and VA-GNRs, which present great agreement with the Langmuir model with the experimental data. The maximum adsorption capacities of MB and OII on VA-GNRs are 280 and 265 mg/g, respectively, which is about three- and twofold larger than VA-SWCNTs with the adsorption capacities of 91.1 and 125 mg/g, respectively. These results confirm that the adsorption capacity of VA-GNRs is much better than VA-SWCNTs.

Separation factor R_L is another fundamentally parametric characteristic of Langmuir model, which is expressed by:

$$R_L = \frac{1}{1 + K_L C_0}, \tag{7}$$

where C_0 is the highest initial concentration of dye used in the study. R_L indicates the adsorption process likely to be among irreversible ($R_L = 0$), favorable ($0 < R_L < 1$), linear ($R_L = 1$), or unfavorable ($R_L > 1$). The smaller R_L values in the Table 3 indicate that the adsorption of MB and OII dyes

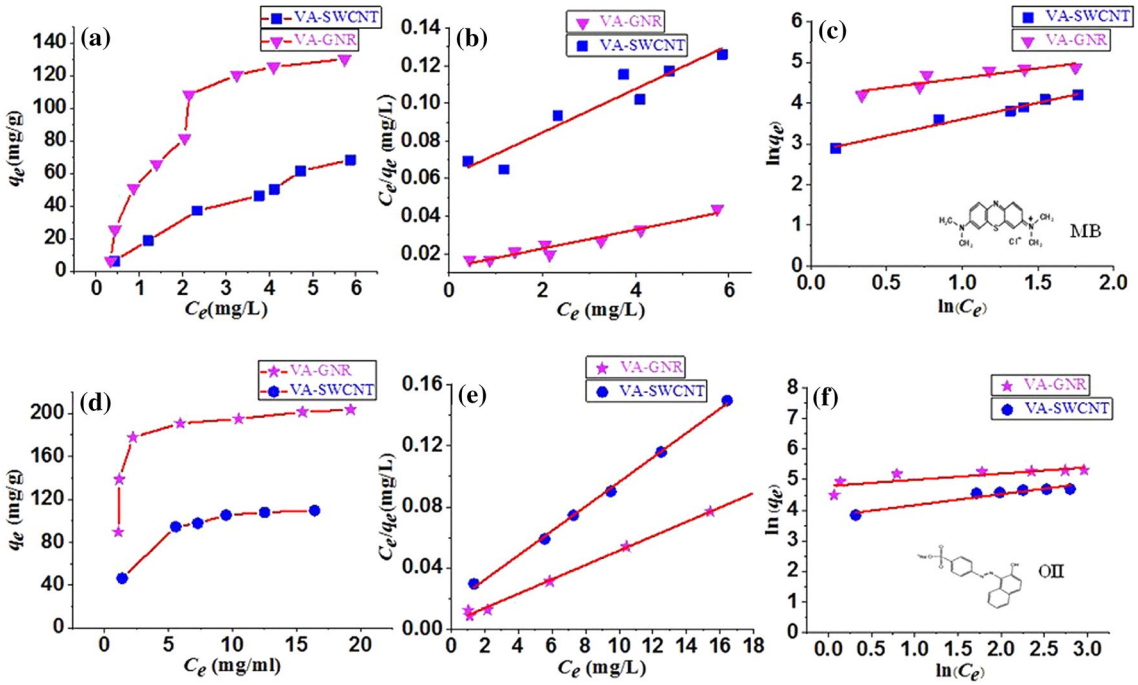

Fig. 7 Adsorption isotherms of **a** MB and **d** OII on VA-SWCNTs and VA-GNRs, respectively. **b**, **e** and **c**, **f** are plots of Langmuir and Freundlich models for the MB and OII adsorption on VA-SWCNTs and VA-GNRs, respectively

Table 3 Parameters of the Langmuir models

Langmuir	MB	SWCNT	GNR	OII	SWCNT	GNR
	q_{max}	91.1	280	q_{max}	125	265
	k_L	6.02	3.13	k_L	0.56	0.62
	R_L	0.28	0.43	R_L	0.55	0.59
	R^2	0.92	0.95	R^2	0.99	0.99

Table 4 Parameters of the Freundlich models

Freundlich	MB	SWCNT	GNR	OII	SWCNT	GNR
	$1/n$	0.81	0.48	$1/n$	0.36	0.20
	K_F	2.57	9.65	K_F	1.23	11.41
	R^2	0.90	0.98	R^2	0.85	0.93

onto both VA-SWCNTs and VA-GNRs are the favorable processes.

The Freundlich model is based upon the simulation of adsorption occurred on multilayer, expressed as:

$$\ln q_e = \frac{1}{n} \ln C_e + \ln K_F, \tag{8}$$

where K_F is a key factor for the adsorption capacity, while $1/n$ is another empirical anisotropic factor, which presents an important information of the offset from linearity fitting for the adsorption data. $1/n$ quantifies the appropriable of adsorption as well as the anisotropic degree of the surface. When $1/n < 1$, it reveals that appropriate adsorption process and also indicates a common Langmuir isotherm model. The relative parameters are demonstrated in Table 4 by fitting the experimental data, as shown in Fig. 7c, f. In our experiment, the quantitative values of $1/n$ are lower than 1 which provides that the adsorption capacity for both MB and OII on VA-SWCNTs and VA-GNRs benefited adsorption processes of the Langmuir model.

4 Conclusion

We have provided the VA-GNRs as a high-efficiency adsorption both valuable for anionic and cationic dyes, which resoundingly cut and unzipped with the atomic hydrogen treatment from VA-SWCNTs. SEM, TEM and AFM analyses have demonstrated that the VA-GNRs formed vertically arranged structures, indicating not only larger active area but also stronger π–π interaction. Besides, it avoids the potential virulence from the extra chemical elements as well as modified and damaged structure of the functional groups. The kinetic studies reveal that the adsorbent experimental data could be fitted by the pseudo second-order rate equation very well. The adsorption capacities of VA-GNRs for MB and OII are 280 and 265 mg/g, respectively, which are much higher than that of initial VA-SWCNTs as well as the literature [23]. The significant improved adsorption capacity strongly suggests that VA-GNRs emerges as great potentially commercial application in engineering for the high efficiency adsorption of both cationic and anionic dyes in the sewage disposal simultaneously. These results indicate that VA-GNRs are a new kind of nano-adsorption materials with the advantages of being cost effective, higher efficient and environmental friendly.

Acknowledgements This work was supported by the National Key Research and Development Program of China [Grant no. 2017YFA0304203]; National Natural Science Foundation of China (NSFC) [Grant nos. 61605104]; PCSIRT [Grant no. IRT_17R70]; 111 project [Grant no. D18001] and Scientific and Technological Innovation Programs of Higher Education Institutions in Shanxi [Grant no. 201802008].

References

1. Eliasson J (2015) The rising pressure of global water shortages. Nature. https://doi.org/10.1038/517006a
2. Ali I (2012) New generation adsorbents for water treatment. Chem Rev 112:5073–5091. https://doi.org/10.1021/cr300133d
3. Yagub MT, Sen TK, Afroze S, Ang HM (2014) Dye and its removal from aqueous solution by adsorption: a review. Adv Colloid Interface 209:172–184. https://doi.org/10.1016/j.cis.2014.04.002
4. Sun H, Cao L, Lu L (2011) Magnetite/reduced graphene oxide nanocomposites: one step solvothermal synthesis and use as a novel platform for removal of dye pollutants. Nano Res 4:550–562. https://doi.org/10.1007/s12274-011-0111-3
5. Seshadri S, Bishop PL, Agha AM (1994) Anaerobic/aerobic treatment of selected azo dyes in wastewater. Waste Manag 14:127–137. https://doi.org/10.1016/0956-053X(94)90005-1
6. Davis RJ, Gainer JL, O'Neal G, Wu IW (1994) Photocatalytic decolorization of wastewater dyes. Water Environ Res 66:50–53. https://doi.org/10.2175/WER.66.1.8
7. Kim TS, Song HJ, Dar MA, Lee HJ, Kim DW (2018) Fast adsorption kinetics of highly dispersed ultrafine nickel/carbon nanoparticles for organic dye removal. Appl Surf Sci 439:364–370. https://doi.org/10.1016/j.apsusc.2018.01.061
8. Yan Y, Zhang M, Gong K, Su L, Zhixin Guo A, Mao L (2005) Adsorption of methylene blue dye onto carbon nanotubes: a route to an electrochemically functional nanostructure and its layer-by-layer assembled nanocomposite. Chem Mater. https://doi.org/10.1021/cm0504182
9. Gupta VK, Agarwal S, Saleh TA (2011) Chromium removal by combining the magnetic properties of iron oxide with adsorption properties of carbon nanotubes. Water Res 45:2207–2212. https://doi.org/10.1016/j.watres.2011.01.012
10. Saleh TA, Gupta VK (2012) Column with CNT/magnesium oxide composite for lead(II) removal from water. Environ Sci Pollut Res 19:1224–1228. https://doi.org/10.1007/s11356-011-0670-6
11. Zhang J, Li F, Sun Q (2018) Rapid and selective adsorption of cationic dyes by a unique metal-organic framework with decorated pore surface. Appl Surf Sci 440:1219–1226. https://doi.org/10.1016/j.apsusc.2018.01.258
12. Xin SC, Yang N, Gao F, Zhao J, Li L, Teng C (2017) Three-dimensional polypyrrole-derived carbon nanotube framework for dye adsorption and electrochemical supercapacitor. Appl Surf Sci 414:218–223. https://doi.org/10.1016/j.apsusc.2017.04.109
13. Gupta VK, Agarwal S, Saleh TA (2011) Synthesis and characterization of alumina-coated carbon nanotubes and their application

for lead removal. J Hazard Mater 185:17. https://doi.org/10.1016/j.jhazmat.2010.08.053
14. Haghdoust S (2012) Comparison of activated carbon, multiwalled carbon nanotubes, and cadmium hydroxide nanowire loaded on activated carbon as adsorbents for kinetic and equilibrium study of removal of Safranine O. Spectrosc Lett 45:500–510. https://doi.org/10.1080/00387010.2011.641058
15. Shirmardi M, Mesdaghinia A (2015) Kinetics and equilibrium studies on adsorption of acid red 18 (Azo-dye) using multiwall carbon nanotubes (MWCNTs) from aqueous solution. J Chem 9:2371–2383. https://doi.org/10.1155/2012/541909
16. Ghaedi M, Khajehsharifi H, Yadkuri AH, Roosta M, Asghari A (2012) Oxidized multiwalled carbon nanotubes as efficient adsorbent for bromothymol blue. Toxicol Environ Chem 94:873–883. https://doi.org/10.1080/02772248.2012.678999
17. Zhao Q, Yang K, Zhang S, Chefetz B, Zhao J, Mashayekhi H, Xing B (2015) Dispersant selection for nanomaterials: insight into dispersing functionalized carbon nanotubes by small polar aromatic organic molecules. Carbon 91:494–505. https://doi.org/10.1016/j.carbon.2015.05.014
18. Yang K, Xing B (2010) Adsorption of organic compounds by carbon nanomaterials in aqueous phase: Polanyi theory and its application. Chem Rev 110:5989–6008. https://doi.org/10.1021/cr100059s
19. Jiang QQ, Lu YF, Huang ZX, Hu JC (2017) Facile solvent-thermal synthesis of ultrathin $MoSe_2$ nanosheets for hydrogen evolution and organic dyes adsorption. Appl Surf Sci 402:277–285. https://doi.org/10.1016/j.apsusc.2017.01.049
20. Wu CJ, Yuan W, Deyab SSA, Zhang KQ (2014) Tuning porous silica nanofibers by colloid electrospinning for dye adsorption. Appl Surf Sci 313:389–395. https://doi.org/10.1016/j.apsusc.2014.06.002
21. Al-Ghouti MA, Khraisheh MA, Ahmad MN, Allen S (2009) Adsorption behaviour of methylene blue onto Jordanian diatomite: a kinetic study. J Hazard Mater 165:589–598. https://doi.org/10.1016/j.jhazmat.2008.10.018
22. Allen SJ, McKay G, Khader KYH (1989) Equilibrium adsorption isotherms for basic dyes onto lignite. J Chem Technol Biotechnol 45:291–302. https://doi.org/10.1002/jctb.280450406
23. Yao Y, Xu F, Chen M, Xu Z, Zhu Z (2010) Adsorption behavior of methylene blue on carbon nanotubes. Bioresour Technol 101:3040–3046. https://doi.org/10.1016/j.biortech.2009.12.042
24. Konicki W, Pelech I, Mijowska E, Jasinska I (2014) Adsorption kinetics of acid dye acid red 88 onto magnetic multi-walled carbon nanotubes-Fe_3C nanocomposite. Clean Soil Air Water 42:284–294. https://doi.org/10.1002/clen.201200458
25. Namasivayam C, Kavitha D (2002) Removal of Congo Red from water by adsorption onto activated carbon prepared from coir pith, an agricultural solid waste. Dyes Pigments 54:47–58. https://doi.org/10.1016/S0143-7208(02)00025-6
26. Khraisheh MAM, Al-Degs YS, Allen SJ, Ahmad MN (2002) Elucidation of controlling steps of reactive dye adsorption on activated carbon. Ind Eng Chem Res 41:1651–1657. https://doi.org/10.1021/ie000942c
27. El Qada EN, Allen SJ, Walker GM (2006) Adsorption of Methylene Blue onto activated carbon produced from steam activated bituminous coal: a study of equilibrium adsorption isotherm. Chem Eng J 124:103–110. https://doi.org/10.1016/j.cej.2006.08.015
28. El Qada EN, Allen SJ, Walker GM (2008) Adsorption of basic dyes from aqueous solution onto activated carbons. Chem Eng J 135:174–184. https://doi.org/10.1016/j.cej.2007.02.023
29. Geng Z, Lin Y, Yu X, Shen Q, Ma L, Li Z, Pan N, Wang X (2012) Highly efficient dye adsorption and removal: a functional hybrid of reduced graphene oxide–Fe_3O_4 nanoparticles as an easily regenerative adsorbent. J Mater Chem 22:3527–3535. https://doi.org/10.1039/C2JM15544C
30. Pang XL, Peng HL, Yang HS, Gao KW, Wu XL, Volinsky AA (2013) Comparative study of methylene blue dye adsorption onto activated carbon, graphene oxide, and carbon nanotubes. Chem Eng Res Des 91:361–368. https://doi.org/10.1016/j.cherd.2012.07.007
31. Nguyen-Phan TD, Pham VH, Shin EW, Pham HD, Kim S, Jin SC, Kim EJ, Hur SH (2011) The role of graphene oxide content on the adsorption-enhanced photocatalysis of titanium dioxide/graphene oxide composites. Chem Eng J 170:226–232. https://doi.org/10.1016/j.cej.2011.03.060
32. Zhang W, Zhou C, Zhou W, Lei A, Zhang Q, Wan Q, Zou B (2011) Fast and considerable adsorption of Methylene Blue dye onto graphene oxide. Bull Environ Contam Toxicol 87:86. https://doi.org/10.1007/s00128-011-0304-1
33. Rodriguez A, Ovejero G, Sotelo JL, Mestanza M, Garcia J (2010) Adsorption of dyes on carbon nanomaterials from aqueous solutions. J Environ Sci Health A 45:1642–1653. https://doi.org/10.1080/10934529.2010.506137
34. Robati D, Mirza B, Ghazisaeidi R, Rajabi M, Moradi O, Tyagi I, Agarwal S, Gupta VK (2016) Adsorption behavior of methylene blue dye on nanocomposite multi-walled carbon nanotube functionalized thiol (MWCNT-SH) as new adsorbent. J Mol Liq 216:830–835. https://doi.org/10.1016/j.molliq.2016.02.004
35. Mishra AK, Arockiadoss T, Ramaprabhu S (2010) Study of removal of azo dye by functionalized multi walled carbon nanotubes. Chem Eng J 162:1026–1034. https://doi.org/10.1016/j.cej.2010.07.014
36. Yao Y, He B, Xu F, Chen X (2011) Equilibrium and kinetic studies of methyl orange adsorption on multiwalled carbon nanotubes. Chem Eng J 170:82–89. https://doi.org/10.1016/j.cej.2011.03.031
37. Xu YQ, Flor E, Kim MJ, Hamadani B, Schmidt H, Smalley RE, Hauge RH (2006) Vertical array growth of small diameter single-walled carbon nanotubes. J Am Chem Soc 128:6560–6561. https://doi.org/10.1021/ja060944+
38. Pint CL, Sun Z, Moghazy S, Xu YQ, Tour JM, Hauge RH (2011) Supergrowth of nitrogen-doped single-walled carbon nanotube arrays: active species, dopant characterization, and doped/undoped heterojunctions. ACS Nano 5:6925–6934. https://doi.org/10.1021/nn201252z
39. Fan X, Peng Z, Yang Y, Zhou H, Guo X (2015) Atomic H-induced cutting and unzipping of single-walled carbon nanotube carpets with teepee structure and their enhanced supercapacitor performance. J Mater Chem A 3:10077–10084. https://doi.org/10.1039/C5TA01426C
40. Zou Y, May PW, Viera SMC, Fox NA (2012) Field emission from diamond-coated multiwalled carbon nanotube "teepee" structures. J Appl Phys 112:044903. https://doi.org/10.1063/1.4748336
41. Geim AK, Novoselov KS (2007) The rise of graphene. Nat Mater 6:183–191. https://doi.org/10.1142/9789814287005_0002
42. Shinde DB, Debgupta J, Kushwaha A, Aslam M, Pillai VK (2011) Electrochemical unzipping of multi-walled carbon nanotubes for facile synthesis of high-quality graphene nanoribbons. J Am Chem Soc 133:4168–4171. https://doi.org/10.1021/ja1101739
43. Talyzin AV, Luzan S, Anoshkin IV, Nasibulin AG, Jiang H, Kauppinen EI, Mikoushkin VM, Shnitov VV, Marchenko DE, Noréus D (2011) Hydrogenation, purification, and unzipping of carbon nanotubes by reaction with molecular hydrogen: road to graphane nanoribbons. ACS Nano 5:5132–5140. https://doi.org/10.1021/nn201224k
44. Morelos-Gómez A, Vega-Díaz SM, González VJ, Tristán-López F, Cruz-Silva R, Fujisawa K, Muramatsu H, Hayashi T, Mi X, Shi Y (2012) Clean nanotube unzipping by abrupt thermal expansion of molecular nitrogen: graphene nanoribbons with atomically

smooth edges. ACS Nano 6:2261–2272. https://doi.org/10.1021/nn2043252
45. Qi YC, Yang MM, Xu WH, He S, Men Y (2017) Natural polysaccharides-modified graphene oxide for adsorption of organic dyes from aqueous solutions. J Colloid Interface Sci 486:84–96. https://doi.org/10.1016/j.jcis.2016.09.058
46. Gupta VK, Kumar R, Nayak A, Saleh TA, Barakat MA (2013) Adsorptive removal of dyes from aqueous solution onto carbon nanotubes: a review. Adv Colloid Interface 193:24–34. https://doi.org/10.1016/j.cis.2013.03.003
47. Abbas AI, Al-Amer AM, Laoui T, Al-Marri MJ, Nasser MS, Khraisheh M, Atieh MA (2016) Heavy metal removal from aqueous solution by advanced carbon nanotubes: critical review of adsorption applications. Sep Purif Technol 157:141–161. https://doi.org/10.1016/j.seppur.2015.11.039
48. An AK, Guo J, Jeong S, Lee EJ, Tabatabai SA, Leiknes T (2016) High flux and antifouling properties of negatively charged membrane for dyeing wastewater treatment by membrane distillation. Water Res 103:362–371. https://doi.org/10.1016/j.watres.2016.07.060

Affiliations

Yan Gao[1,2,3] · Xilong Liang[2,3] · Shuangping Han[2,3] · Liang Wu[1] · Guofeng Zhang[2,3] · Chengbing Qin[2,3] · Shanxia Bao[1] · Qiang Wang[1] · Lele Qi[1] · Liantuan Xiao[2,3]

✉ Yan Gao
ago@sxu.edu.cn

✉ Lele Qi
392864788@qq.com

[1] Department of Physics, Shanxi Datong University, Datong 037009, China

[2] State Key Laboratory of Quantum Optics and Quantum Optics Devices, Institute of Laser Spectroscopy, Shanxi University, Taiyuan 030006, China

[3] Collaborative Innovation Center of Extreme Optics, Shanxi University, Taiyuan 030006, Shanxi, China